Novel Injectable Gallium-based Self-Setting Glass-Alginate Hydrogel Composite for Cardiovascular Tissue Engineering

Owen M. Clarkin[a], Bing Wu[a,b,c,], Paul A. Cahill[d], Dermot F. Brougham[c], Dipanjan Banerjee[b,e], Sarah A. Brady[a], Eoin K. Fox[a], Caitríona Lally[f]*

a. DCU Biomaterials Research Group, Centre for Medical Engineering Research, School of Mechanical and Manufacturing Engineering, Dublin City University, Dublin 9, Ireland.

b. DUBBLE Beamline, European Synchrotron Radiation Facility (ESRF), 71 avenue des Martyrs, CS 40220, Grenoble 38043, France

c. School of Chemistry, University College Dublin, Belfield, Dublin 4, Ireland

d. Vascular Biology and Therapeutic Laboratory, School of Biotechnology, Faculty of Science and Health, Dublin City University, Dublin 9, Ireland.

e. Department of Chemistry, KU Leuven, Celestijnenlaan 200F box 2404, 3001 Leuven, Belgium.

f. Department of Mechanical and Manufacturing Engineering, School of Engineering and Trinity Centre for Bioengineering, Trinity College Dublin, Dublin 2, Ireland.

17

18   **ABSTRACT**

19   Composite biomaterials offer a new approach for engineering novel, minimally-invasive scaffolds

20   with properties that can be modified for a range of soft tissue applications. In this study, a new

21   way of controlling the gelation of alginate hydrogels using Ga-based glass particles is presented.

22   Through a comprehensive analysis, it was shown that the setting time, mechanical strength,

23   stiffness and degradation properties of this composite can all be tailored for various applications.

24   Specifically, the hydrogel generated through using a glass particle, wherein toxic aluminium is

25   replaced with biocompatible gallium, exhibited enhanced properties. The material's stiffness

26   matches that of soft tissues, while it displays a slow and tuneable gelation rate, making it a suitable

27   candidate for minimally-invasive intra-vascular injection. In addition, it was also found that this

28   composite can be tailored to deliver ions into the local cellular environment without affecting

29   platelet adhesion or compromising viability of vascular cells in vitro.

30

1. Introduction

The growing demand for minimally-invasive surgical procedures, combined with increased use of tissue engineering (TE) strategies has led to a requirement for extremely low viscosity injectable TE scaffolds (Balakrishnan, Joshi, Jayakrishnan, & Banerjee, 2014; Buwalda et al., 2014). Such injectables should be capable of passing through fine microcatheters (<0.38 mm internal diameter) and yet forming a solid matrix in vivo. Traditionally, TE scaffolds are pre-formed prior to implantation. However, this is not a suitable approach for minimally-invasive procedures, which can reduce cost as well as morbidity, and hence have grown in prevalence (Bragg, Vanbalen, & Cook, 2005). Acellular scaffolds, tailored for minimally-invasive procedures, can provide a rich environment for resident cellular proliferation while offering a shorter regulatory route to clinical application (Li, Kaplan, & Zreiqat, 2014). For other applications where there is limited blood supply and limited resident cell proliferative capacity, a cell-seeded graft may be the only viable solution. Hence, novel materials for acellular scaffolds used in minimally-invasive procedure are of great interest to both acellular and cell-based therapies.

Bioactive glasses have been shown to induce cellular proliferation due to the release of beneficial inorganic ions, which can encourage the development of natural extracellular matrix (Azevedo et al., 2015; Henstock, Canham, & Anderson, 2015). However, to date, the advantages of this form of ion release have been limited to hard tissue orthopaedic applications. On the other hand, a range of injectable polymeric formulations have been investigated for soft tissue applications, but many contain toxic monomers, activators and free radicals (Bearat, Lee, Valdez, & Vernon, 2011; Kadouch, Vos, Nijhuis, & Hoekzema, 2015). The elastic modulus ranges of currently available soft tissue augmentation materials do not match those of augmented tissues, examples include fibrin (50 Pa), Matrigel™ (30-120 Pa), type I collagen gels (20-80 Pa for 1-3 mg/ml), N-

54   isopropylacrylamide (100-400 Pa) and PEG (1-3 kPa) (Ravichandran, Venugopal, Sundarrajan,

55   Mukherjee, & Ramakrishna, 2012). Compared to tissues such as human cardiac tissue (50 kPa)

56   (Omens, 1998) and carotid artery (160-390 kPa) (Messas, Pernot, & Couade, 2013), these

57   materials are considerably less stiff and so are unsuitable as mechanical supports for tissue

58   regeneration. Additionally, many biomaterials have fast and uncontrolled gelation rates, which

59   increase the likelihood of blocking blood flow following injection in vivo, causing tissue necrosis

60   (Eschenhagen, Didie, Heubach, Ravens, & Zimmermann, 2002). For intra-vascular defects, such

61   as intracranial aneurysms, arteriovenous malformations and dural fistula, two commercial

62   polymers are widely used. One is cyanoacrylate glues, and the other is an ethylene-vinyl alcohol

63   copolymer dissolved in dimethyl sulfoxide (EVOH/DMSO). In the first case, this glue sets

64   immediately on contact with blood, allowing little or no time for placement and manipulation (Jin

65   et al., 2011). In the second case, DMSO must first wash out before the polymer precipitates which

66   can result in significant implant migration (9-33% of cases) (Murayama, Vinuela, Tateshima,

67   Vinuela, & Akiba, 2000).

68   Glass polyalkenoate cements (GPCs), commonly used in dentistry, are produced by mixing a

69   calcium-alumino-silicate glass with a poly(alkenoic acid). To form a composite, ions are released

70   from the glass phase, which crosslink the polyacid. In these formulations, aluminium (Al) is

71   predominantly in four-fold coordination, substituting for silicon in the basic SiO_4 glass unit,

72   resulting in highly connected networks with controlled reactivity. The extra negative charge on the

73   AlO_4 tetrahedra is balanced by network modifying cations, such as Ca^{2+} (Wilson & Nicholson,

74   1993). This acid labile structure allows the glass to maintain a large quantity of ions without

75   excessive reactivity. However, leaching of aluminium from these materials has been shown to have

76   neurotoxic effects and inhibit bioactivity (Brook & Hatton, 1998). Attempts have been made to

77 produce GPCs without Al in the glass phase, most notably replacing it with iron or zinc. However,

78 redox active Fe can form toxic radicals, while Zn disrupts the glass network, resulting in a weaker,

79 faster setting material (Boyd, Clarkin, Wren, & Towler, 2008).

80   Gallium (Ga) may be a viable alternative to Al in the glass structure. Ga is not redox-active under

81 physiological conditions and can serve to reduce reactive oxygen species (ROS) (Bearat et al.,

82 2011). Ga should form tetrahedra in silica glasses similar to Al and should be acid labile, reacting

83 at low pH to release di- and tri-valent ions in a controlled manner (Shelby, 1994). The resulting

84 surface ion-depleted silica gels exhibit slow diffusion-controlled release of ions into the

85 surrounding aqueous environment, a property attributed to ongoing crosslinking of hydrogels.

86 Previously, this property has been used to control crosslinking of poly(acrylic acid) in GPCs but

87 this results in stiff, low water content, hydrogels, unsuitable for soft tissue applications. (Wren,
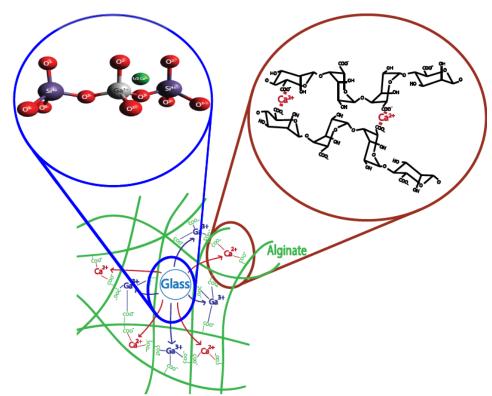
88 Coughlan, Placek, & Towler, 2012)

89

90   **Figure 1:** Schematic representing the structure of the novel composite hydrogel.

91   In this study, we describe novel glass formulations ($23CaO-xGa_2O_3-(18-x)Al_2O_3-33SiO_2-$

92    $11P_2O_5-15CaCl_2$, where x=0, 6, 12, 18). The glass incorporates large quantities of di- and tri-valent

93   ions in order to fully crosslink the alginate polymer, while limiting ion availability so as to allow

94   control over the setting kinetics of the gel. This property is provided by the inclusion of Ga into

95   the composition, as a replacement for Al, which produces a charge balanced, acid-labile tetrahedral

96   structure, as depicted in **Fig. 1**. An alginate matrix was selected because of its excellent

97   injectability through microcatheters, its chemical and mechanical diversity and its excellent

98   biocompatibility (Grover, Braden, & Christman, 2013). Previous studies have utilised an

99   alginate/calcium chloride mix, wherein no control of the setting reaction was demonstrated and

100   which required complicated double lumen microcatheters to prevent setting of the gel during

101   delivery (Becker & Kipke, 2002). In our case, the control of the glass chemistry and particle size

102   enables control over the setting kinetics of the alginate gel that results in ongoing strengthening of

103   the gel over a period of days an additional advantage which has not previously been reported for

104   alginates. (Lee & Mooney, 2012)

105   **2. Experimental**

106   **2.1 Glass Synthesis**

107   Four glass formulations (AL100, AL067, GA067 and GA100) were produced, with increasing

108   (Ga/(Al+Ga) ratios (**Table 1**). Glasses were prepared by weighing out analytical grade reagents

109   (Sigma-Aldrich, Dublin, Ireland) and were mixed in a rotor (10 minutes). Compositions were fired

110   (1480 ˚C, 1 h) in 10% Rhodium/Platinum crucibles and shock quenched into water. The resulting

111   frit was dried (100 ˚C, 1 h) and ground using a vibratory mill to <63 μm. The glass powder was

112   further ground in methanol in an attrition mill using 1 mm alumina media. Methanol was

113   subsequently evaporated to retrieve the final glass powder.

114   **2.2 Network Connectivity Calculations**

115   The network connectivity (NC) of the glasses was calculated with Eqn. (1) using the molar

116   compositions of the glass.

117
$$NC = \frac{No.\ BOs - No.NBOs}{Total\ No.Bridging\ Species} \tag{1}$$

118   Where BO means Bridging Oxygens, NBO is Non-Bridging Oxygens.

119   **2.4 Purification of Potassium Alginate**

120   Purification of crude sodium alginate (Sigma Aldrich, Wicklow, Ireland) was carried out in a

121   similar fashion to published procedures and aimed to remove protein and endotoxin contamination

122   (Dusseault et al., 2006; Jork et al., 2000; Klock et al., 1994; Zimmermann et al., 1992). Briefly,

123   sodium alginate was dissolved in saline, filtered over, successively, 2.5 and 0.45 μm filters,

124   precipitated as alginic acid by reducing the pH to 1.5.(Brady, Fox, Lally, & Clarkin, 2017) The

125   precipitate was washed with chloroform and 1-butanol three times before re-dissolving by raising

126   the pH to 7.0. The solution was again washed with chloroform and 1-butanol and separated by

127   centrifugation. Finally, the potassium alginate solution was precipitated in absolute ethanol,

128   washed in diethyl ether, frozen (-80 ˚C) and lyophilized.

129   **2.3 Potassium Alginate Chemical Analysis**

130   Gel permeation chorography (GPC) and nuclear magnetic resonance spectroscopy (^{1}H-NMR)

131   were carried out as follows in order to characterize the alginates produced. GPC was found using

132   a liquid chromatography system (Agilent 1200, Agilent, USA) equipped with a Suprema Linear

133   GPC column (PSS, Germany). The mobile phase used consisted of 0.1M disodium hydrogen

134   phosphate containing 0.5g/l of sodium nitrate buffered to pH 9. All samples were injected at a

135   concentration of 1mg/ml, at a flow rate of 0.5ml/min. Pullulan standards were injected to construct

136   calibration curves. ^{1}H-NMR of the potassium alginate was tested using a modified version of the

137 standard ASTM F2259–03. The alginate solution was prepared by mixing the alginate to a 0.1%

138 (w/v) in DI. HCl was used to bring the alginate pH to 5.6 and the alginate solution was stored in a

139 water bath at 100°C for 1 hour. HCl was used to further adjust the pH of the alginate to 3.8. The

140 solution was stored again in a water bath at 100°C for 30 minutes. The pH was then raised to 7

141 using NaOH and the alginate was freeze dried. The alginate was then dissolved in 5ml of 99%

142 D_2O and freeze dried overnight. 12mg of alginate was dissolved in 1ml of D_2O and placed in a

143 NMR tube. The NMR of the alginate was tested using a Bruker Advance 400 (Bruker,

144 Massachusetts, USA) at 80°C. 64 scans were carried out using a 2s relaxation delay. The M/G

145 ratios were then calculated as per ASTM F2259-03.

2.5 Hydrogel Production

147 A 2 wt% potassium alginate solution was produced by mixing dry, sterile filtered potassium

148 alginate with sterile filtered (<0.22 µm) water. Glass powder was sterilised under UV light for 15

149 minutes and a 9.2 wt% glass solution was produced by mixing with sterile filtered water and

150 agitating for 30 seconds. Hydrogel samples were then produced by mixing 600 µl of glass solutions

151 with 0.05 g of UV sterilized glucono-δ-lactone (GDL) for 10 seconds, followed by mixing with

152 600 µl of alginate solution for a further 60 seconds.

2.7 Working and Setting Time Determination

154 To test for working and setting time, the composition is mixed for 1 minute before being placed

155 in a stainless steel mould (ϕ=10 mm, h=5 mm) sitting on a large steel block which was pre-heated

156 to 37˚C. The hydrogel was then indented vertically using a 20 g weight with a 6 mm diameter

157 indenter. The working time (WT) is defined as the time at which the mould can be lifted and held

158 in the air for 10 s without the sample flowing out. The setting time (ST) is defined as the time at

159   which a mark, formed by a certain indenter placement for 10 seconds, does not recover within one

160   minute following indentation.

161   **2.8 Mechanical Testing**

162   Five samples (n=5) were produced for compression testing by mixing samples for 1 minute

163   before placing into moulds (ϕ=9.00 mm, h=15.00 mm). Samples were covered with an acetate

164   sheet and allowed to set for 60 minutes before being placed into 20 ml of Dulbecco's Modified

165   Eagle Medium containing 1 vol.% penicillin streptomycin. Samples were tested using a 5kN Zwick

166   BT1-FR005TN test machine fitted with a 500N load cell and parallel plate platens. Samples were

167   loaded at 2 mm/min to failure and data was recorded using TestXpert software (v.11.02) (Zwick,

168   Ulm, Germany). Peak stress and elastic modulus prior to failure was determined (c.30-50% strain).

169   **2.9 Elution MTT Assay**

170   MTT Elution Assays were carried out using Bovine aortic smooth muscle cells (BASMCs) and

171   bovine aortic endothelial cells (BAECs) as per ISO 10993-5, briefly described here. A composite

172   hydrogel sample was produced and set in cylindrical silicone moulds (ϕ=15 mm, h=1 mm).

173   Samples were left to set for 1 h before being placed in 2.75 ml of DMEM cell culture media (as

174   per ISO10993-5) supplemented with 10 vol% fetal calf serum and 1 vol.% penicillin-streptomycin

175   (Sigma Aldrich, Wicklow, Ireland) at the bottom of 24 well plates. Samples were incubated for

176   48 h (37 ˚C, 5 % CO_2). Elution media was gently removed and filtered through a 0.22 μm sterile

177   filter. At this point some media was removed for ion analysis (see **SI**). BASMCs and BAECs were

178   cultured using Dulbecco's modified Eagle's medium (DME, cell passage number from 3 to 6).

179   Cells were seeded at 40,000 cells per 100 μl of media in 96 well plates and incubated until they

180   formed a sub-confluent monolayer (37 ˚C, 5 % CO_2). Media was then aspirated off and cells were

181   placed in varying concentrations of elution media (0, 20, 40, 60, 80, 100 vol%) and incubated for

182   24 h. MTT solution was produced by dissolving 50 mg of Thiazolyl Blue Tetrazolium Bromide in

183   10 ml of sterile PBS and was filtering through a 0.22 μm sterile filter.(Hong et al., 2012) Following

184   incubation, elution media was aspirated off, cells were washed with 100 µl of PBS (Ca^{2+}, Mg^{2+}

185   free), 100 µl of MTT solution was placed into each well and incubated for 5 h (37 ˚C, 5 % CO_2).

186   The MTT solution was then aspirated off, 100 µl of DMSO was added to each well plate and then

187   shaken for 15 s and incubated at room temperature for 10 mins. Optical densities were recorded at

188   540 nm with a reference wavelength at 630 nm. Cell viabilities were calculated as a percentage of

189   untreated control cells using the following equation:

190    $$Cell\ Viability\ (\%) = \frac{Absorbance_{540nm}\ of\ treated\ cells}{Absorbance_{540nm}\ of\ untreated\ cells} \times 100 \qquad (2)$$

191   **2.10 DAPI and phalloidin Staining**

192   6 well plates of BASMCs were seeded and treated as described above but following 24 h

193   incubation cells were rinsed in 1% bovine serum albumin in PBS and fixed for 15 minutes in a 4%

194   formaldehyde, 2% sucrose PBS solution. Cells were permeabilized with a 0.5% Triton X-100

195   solution and stained with a 50 µg/ml phalloidin solution and a 1:1000 DAPI solution. Fluorescence

196   microscopy was carried out on an Olympus BX51 (Tokyo, Japan) at excitation wavelengths of 358

197   and 495 nm. Images were captured using CellF software (Olympus) and cell counts were carried

198   out using Image J (National Institutes of Health, Maryland, USA).

199   **3. Results and Discussion**

200   **3.1 Primary physical characterization of the glasses and alginate**

201   A series of glasses with increasing mole fraction of Ga were prepared, the compositions are

202   given in Table 1. X-ray diffraction patterns indicate that all glasses (AL100-GA100) are

203   amorphous in nature. Particle size of all glasses were determined by laser diffraction and found to

204   be similar in all cases, ranging 1-20 μm with volume mean diameters of 4.3 to 5.3 μm. It was

205   found that the glass transition temperature (T_g) is c. 670 °C, and does not change significantly

206   (p>0.05) when Al is entirely replaced by Ga, indicating that the glass network connectivity is

207   similar in both cases (see **Fig. S8**). A slight mixed oxide effect is observed for the measured T_g

208   values of the intermediate mixed oxides of Ga_2O_3/Al_2O_3; which has been observed in other studies

209   of mixed oxide glasses (Cramer, Gao, & Funke, 2005; Kjeldsen et al., 2013), suggesting a

210   microscopic homogeneous mixing. A helium pycnometer was used to obtain density data for the

211   glass powders. An approximately linear increase in density of 0.14 $g^{-1}cm^3$ (R^2=0.95) is observed

212   with increased Ga/(Al+Ga) ratio (see **Fig. S8**). As expected, this systematic increment is due to

213   the heavier atomic mass of Ga which also implies a similarity in the glass network connectivity.

214

215   **Table 1:** Glass series compositions.

Glass:	Oxides (mole fraction)					
	SiO_2	Al_2O_3	Ga_2O_3	CaO	P_2O_5	$CaCl_2$
AL100	0.33	0.18	0.00	0.23	0.11	0.15
AL067	0.33	0.12	0.06	0.23	0.11	0.15
GA067	0.33	0.06	0.12	0.23	0.11	0.15
GA100	0.33	0.00	0.18	0.23	0.11	0.15

216

217   To evaluate the chemical environment of the glasses, solid-state NMR and Extended X-ray

218   Absorption Fine Structure (EXAFS) were recorded for all the samples. It was found that there are

219   three different aluminium coordination sites, and the Al site distribution changes on substituting

220   with Ga, suggesting a different site preference for the latter ion. On the other hand, a distorted

221   tetrahedral coordination environment for Ga was found in all the Ga-containing samples (detailed

222   analyses see **SI**).

The results of network connectivity (NC) calculations are outlined in **Table 2** (for detailed calculation see **SI**). In these calculations silicon is assumed to form four coordinated tetrahedra with oxygen, whereas the relative aluminium coordination is calculated based on curve fitting of the ^{27}Al-MAS-NMR spectrum. For each aluminium tetrahedron formed it is assumed that half of one Ca^{2+} is required for charge balancing purposes. Phosphorous, as indicated by ^{31}P-MAS-NMR, is assumed to form only a pyrophosphate (Q^1) coordination, wherein the phosphate is bound to only one other phosphate in the network, forming one bonding oxygen (BO) and three non-bonding oxygens (NBOs). The glass network is found to form a Q^3 structure with NC value 3.34-3.57. The ^{29}Si-NMR data indicates a broad peak, typical of silica glass structures, with a δ_{iso} of -80 ppm. For the calculated NC value (Q^3) we would expect a δ_{iso} value closer to -90 ppm. (Stamboulis, Law, & Hill, 2004) This overestimation may be due to a shortage of calcium ions available for tetrahedra charge compensation, resulting in increased network disruption.

Table 2: Glass series coordination and network connectivity calculations.

Glass	SiO_2[a]	Al_2O_3			Ga_2O_3	P_2O_5 (Q^1)	CaO	$CaCl_2$	NC[b]
		IV	V	VI	IV				
AL100	0.33	0.10098	0.04212	0.03690	0.00	0.11	0.23	0.15	3.02
AL067	0.33	0.06972	0.04140	0.00888	0.06	0.11	0.23	0.15	3.34
GA067	0.33	0.02418	0.02982	0.00600	0.12	0.11	0.23	0.15	3.41
GA100	0.33	0.00000	0.00000	0.00000	0.18	0.11	0.23	0.15	3.57

[a]The compositions given are from the glass formulation (**Table 1**).

[b]Assumptions are made that; (i) silicon forms tetrahedra (4BO, 0NBO) if no free modifying cations are present, (ii) phosphorous forms Q2 metaphosphate units (as indicated by NMR analysis), combining with calcium to form discrete $Ca_2O_7P_2$ that do not interact with the network, (iii) gallium forms tetrahedra (4BO, 0NBO), as indicated by EXAFS, (iv) Al(IV):Al(V):Al(VI) ratios are from NMR analysis and subsequent fitting, where Al(IV) contributes 4BO, 0NBO, Al(V) contributes 4BO, 1NBO, Al(VI) contributes 3BO, 3NBO, (V) uncoordinated Ca^{2+} and Cl^- contribute to one NBO each.

244   The purified potassium alginate was chemically analyzed using gel permeation chromatography

245   (GPC) and nuclear magnetic resonance spectroscopy (^{1}H-NMR). The average molecular weight

246   (MW) of the potassium extracted from GPC analyses was found around 700kDa. (**Fig. S3**) ^{1}H-

247   NMR analyses of the potassium alginate were used to determine the guluronic acid (F_G),

248   mannuronic acid (F_M) and alternating block (F_{GM}) fractions, which were calculated to 1.7 (M/G

249   ratio) as per ASTM F2259 – 03. (**Fig. S4**).

250

251   **3.2 Composite gel formation and performance**

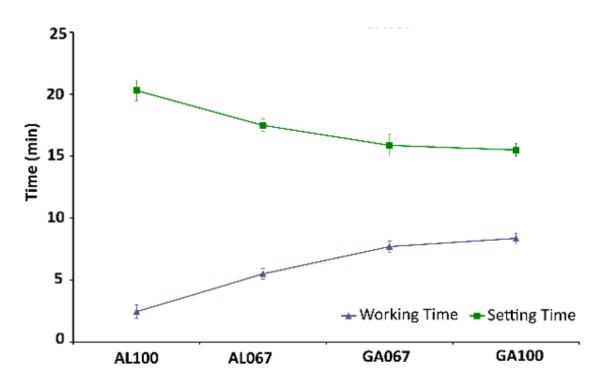252   **3.2.1 Gel formation.**

253

255   **Figure 2**. Working and setting times of the alginate composites.

256   As can be observed from **Fig. 2**, replacing Al with Ga in the glass results in a change in the gel

257   formation; substitution increases the working time (WT) by 77% and decreases the setting time

258   (ST) by 43%, *i.e.* it improves the '*snap-set*' of the gel. This would aid placement of the gel in vivo

259   and prevent '*wash-out*' in a blood flow environment. These requirements have been identified as

260   critical for development of next generation extracellular matrix substitutes (Vernon, 2011). The

261   increased WT and decreased ST of the hydrogel are reflective of the increased stability in the glass

262   structure (higher NC) and higher affinity for alginate binding to Ga over Al, due to its larger ionic

263   radius (Hill & Brauer, 2011). The alginate gelation rate is a critical factor in controlling gel

264   uniformity and strength, with slower gelation producing more uniform structures and greater

265   mechanical integrity (Kuo & Ma, 2001). Other gelation agents in use with alginate gels are usually

266   inorganic salts, however each one of these has its own disadvantages (detailed discussion see **SI**).

267   On the other hand, both ultimate compression strength and elastic modulus increase significantly

268   ($p<0.05$) and approximately linearly (R^2=0.90, 0.96, respectively) with increasing Ga content as

269   shown in **Fig. 4**. With the gallium-only gel exhibiting compression strength and elastic modulus

270   approximately 4 times those of the aluminium-only gel, as noted above Ga is expected to exhibit

271   a higher degree of alginate crosslinking (Haug & Smidsrod, 1970; Yang et al., 2013).
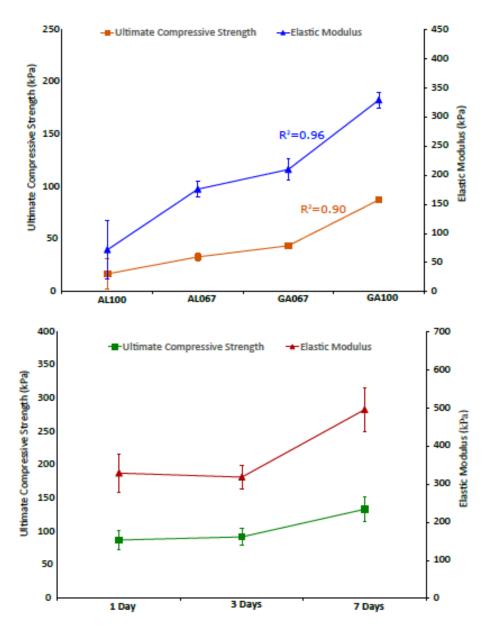
Figure 4: Ultimate compressive strength and elastic modulus of A) composites produced from the different glass compositions and B) GA100 after various time points soaking in DMEM.

3.2.2 Development of properties.

Considering the physical properties of the gels together; the increase in WT with Ga content suggests a less reactive glass, i.e. Ga either reduces the effective rate of ion delivery to the alginate sites, and/or the released ions crosslink the gel less effectively. However, the latter is not consistent

279 with the increased strength of the final Ga containing gels, Figure 4. Stronger gels are anticipated,

280 as Ga is expected to exhibit a higher degree of alginate crosslinking than Al, given its increased

281 ionic radius (Haug & Smidsrod, 1970; Yang et al., 2013). The decrease in ST with Ga content can

282 also be explained by the formation of stronger crosslinks. So it is far more likely that Ga

283 substitution reduces the effective ion delivery rate.

284 It should be noted that the slight downfield shifts observed in ^{31}P and ^{29}Si with increasing Ga

285 content, suggest slightly higher negative charge on Ga than on Al, indeed Ga^{3+} is generally

286 described as the more basic ion. This might render the Ga glasses more susceptible to acid attack

287 (note that all the compositions are hydrolytically stable in the absence of GDL.

288 For blood contact applications, such as treatment of cerebral aneurysms, the gel's compressive

289 strength would need, at a minimum, to be capable of withstanding hypertensive blood pressure

290 (140 mm Hg, or 19 kPa) (Brady et al., 2017). After 1 day of incubation, AL100 has a mean

291 compressive strength of only 17.0 kPa. However, all the other gels exhibit a compressive strength

292 greater than hypertensive blood pressure at 1 day of incubation, with GA100 exhibiting strengths

293 over four times the minimum requirement for this application. In comparison, ethylene vinyl

294 alcohol (EVOH) based polymers (12wt% EVOH, 88% DMSO), used in arterial applications

295 exhibit a strength of 22 kPa after 1 day of immersion in DMEM (**Fig. S5**).

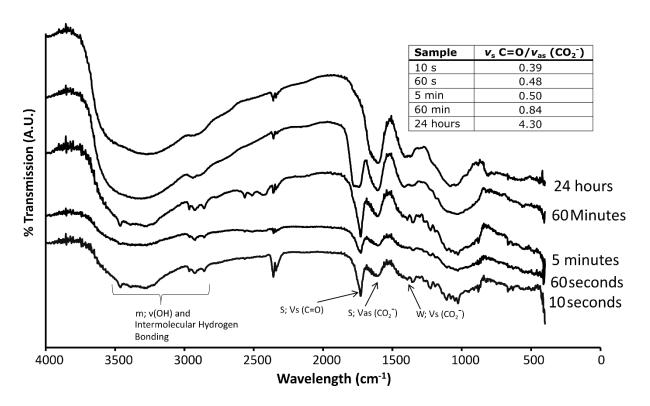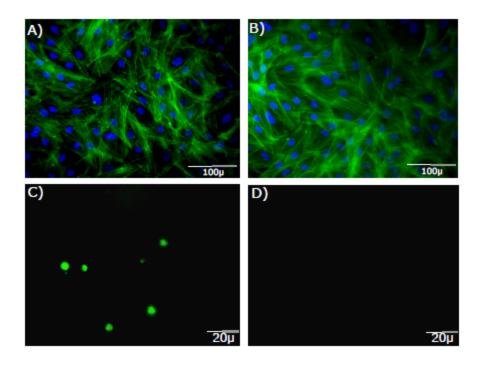| Sample	v_s C=O/v_{as} (CO_2^-)
10 s	0.39
60 s	0.48
5 min	0.50
60 min	0.84
24 hours	4.30

296

Figure 5: FTIR of GA100 at various time points during setting.

298   Turning to the development of the physical properties with time, Fourier Transform Infrared

299   (FTIR) spectrum data (**Fig. 5**) recorded during the setting of the gallium-only gel indicates a first

300   order kinetics reaction which is on-going for up to 24 hours. However, mechanical data indicates

301   a more prolonged setting process, with both strength and elastic modulus increasing significantly

302   ($p<0.05$) with time up to 7 days (the maximum time period examined). This on-going reaction is

303   likely a result of increased crosslink density due to continued release of ions from the glass phase.

304   This is highly unusual for alginate-based gels, particularly for those stored in saline solutions (e.g.

305   DMEM, as in this case). Calcium alginates tend to degrade in saline solution due to the exchange

306   of calcium ions for sodium and potassium ions, weakening the gels and limiting long-term stability

307   under physiological conditions (Lee & Mooney, 2012). It is expected that this effect will help to

308   maintain structural integrity of the gel in vivo.

309   **3.2.3 Impact in cellular environment.**

17

310   The GA100 gel was analysed by ICP-AES, and shown to release significant quantities of

311   potassium (6.98 mM), gallium (3.79 mM) and calcium (3.54 mM), as well as minor quantities of

312   silicon (1.14 mM) into DMEM at 37°C over 48 hours. Note that the ions released are < 1% of the

313   ion content of the glass phase. Release of chlorine and phosphorous was below detectable limits

314   (<0.01 ppm). After 48 hours of ion release, the neat eluent did not cause any significant change in

315   cell viability, for either BASMCs or BAECs (**Fig. 6E**). DAPI cell counts also indicated no

316   significant difference in cell numbers between untreated cells and cells treated with 48 hours

317   DMEM elution media (**Fig. 6A** & **Fig. 6B**). In comparison, an EVOH/DMSO composition

318   exhibited significant reduction in cell viability over 48 hours (see **Fig. S6**). Al has been shown to

319   inhibit activity of the enzyme superoxide dismutase (SOD) in vitro, resulting in increased

320   concentration of ROS. On the other hand, Ga has been shown to significantly enhance SOD

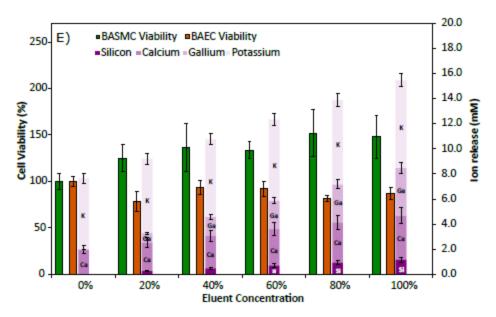321   activity resulting in decreased ROS (Beriault et al., 2007).

Figure 6: DAPI and phalloidin stained BASMCs treated with A) 48 hr eluent and B) control media; fluorescent microscopy (488 nm) of C) Ti6Al4V control sample immersed in platelet suspension for 60 minutes, D) GA100 hydrogel sample and E) ion release and cell viability (BASMCs & BAECs) of GA100 hydrogel.

327   We suggest that Ga ions present in the medium may reduce oxidative stress on cells which is

328   known to be present in the normal cell culture environment (Halliwell, 2003). This mechanism

329   may underpin the observed high cytocompatibility of the glass-alginate gel eluent. This gallium

330   release may also act to inhibit the cell death observed in many cell seeded scaffolds in vivo and

331   reduce the inflammatory response observed in Ca^{2+} releasing calcium alginate gels (Chan &

332   Mooney, 2013).

333   No platelet adhesion was observed on the hydrogel in vitro under static condition (for detailed

334   experimental protocol, see **SI**). Platelets are clearly observed attached to the surface of the titanium

335   positive control samples, as observed using high vacuum and environmental SEM, and

336   fluorescence microscopy (**Fig. 6C**). No attached platelets were observed on the surface of the

337   GA100 hydrogel sample when observed using the same techniques (see **Fig. 6D**). The retention of

338   this favourable attribute in the composite is probably due to the hydrophilic nature of the systems,

339   and is consistent with the expectation for alginate-based hydrogels (Thankam & Muthu, 2013).

340   The use of gallium as opposed to calcium for crosslinking may also prevent initiation of the

341   coagulation cascade (Suzuki et al., 1998). Critically, the glass particles present in the gel do not

342   encourage platelet adhesion under standard incubation conditions.

343   **4. Conclusions**

344   In this study we produced a novel glass formulation, based on glass polyalkenoate cements,

345   whereby neurotoxic Al in the glass phase was replaced by Ga. The Ga in the glass was shown to

346   form predominantly tetrahedral structures, allowing inclusion of high di- and tri- valent ion

347   content, yet maintaining high network connectivity, resulting in a slowly setting glassy silicate

348   network. As a result, the glass reacted sufficiently slowly with an alginate polymer solution to be

349   injectable, while setting within 30 minutes of mixing. This is in stark comparison to commercially

350 available cyanoacrylates, or EVOH based formulations, which set immediately upon contact with

351 blood, making correct placement difficult. Bonds continued to develop in the gel up to 24 hours

352 after setting, as shown by FTIR analysis, and the strength of the gel continued to increase with

353 time up to 7 days. Substitution of Al by Ga lengthened working time, shortened setting time and

354 increased strength and stiffness moving the material into the suitable range for blood contact, and

355 arterial and cardiac tissue engineering applications. The Ga containing hydrogels did not induce

356 any platelet adhesion or activation and eluents from the gels did not result in significant cell death

357 for either BASMCs or BAECs. The provision of controlled gelation and retention of gel strength

358 over time in an aqueous environment, as well as high biocompatibility, gives these novel

359 composite hydrogels exciting potential for applications in minimally-invasive delivery in blood

360 contact environments, and for future cell-based tissue engineering applications.

361 **ASSOCIATED CONTENT**

362   **Supporting Information**. ^{27}Al-MAS-NMR, ^{1}P-MAS-NMR, ^{1}H-NMR, gel permeation

363 chromatography, injectability, compression, EXAFS fitting parameter and cytotoxicity data.

364 **AUTHOR INFORMATION**

365 **Corresponding Author**

366 * bing.wu@esrf.fr

367 **Author Contributions**

368 The manuscript was written through contributions of all authors. All authors have given approval

369 to the final version of the manuscript.

370 **Funding Sources**

375 REFERENCES

376 Azevedo, M. M., Tsigkou, O., Nair, R., Jones, J. R., Jell, G., & Stevens, M. M. (2015). Hypoxia
377   Inducible Factor-Stabilizing Bioactive Glasses for Directing Mesenchymal Stem Cell
378   Behavior. *Tissue Engineering Part A,* 21(1-2), 382-389.
379 Balakrishnan, B., Joshi, N., Jayakrishnan, A., & Banerjee, R. (2014). Self-crosslinked oxidized
380   alginate/gelatin hydrogel as injectable, adhesive biomimetic scaffolds for cartilage
381   regeneration. *Acta Biomater,* 10(8), 3650-3663.
382 Bearat, H. H., Lee, B. H., Valdez, J., & Vernon, B. L. (2011). Synthesis, Characterization and
383   Properties of a Physically and Chemically Gelling Polymer System Using Poly(NIPAAm-
384   co-HEMA-acrylate) and Poly(NIPAAm-co-cysteamine). *Journal of Biomaterials Science-
385   Polymer Edition,* 22(10), 1299-1318.
386 Becker, T. A., & Kipke, D. R. (2002). Flow properties of liquid calcium alginate polymer injected
387   through medical microcatheters for endovascular embolization. *Journal of Biomedical
388   Materials Research,* 61(4), 533-540.
389 Beriault, R., Hamel, R., Chenier, D., Mailloux, R. J., Joly, H., & Appanna, V. D. (2007). The
390   overexpression of NADPH-producing enzymes counters the oxidative stress evoked by
391   gallium, an iron mimetic. *Biometals,* 20(2), 165-176.
392 Boyd, D., Clarkin, O. M., Wren, A. W., & Towler, M. R. (2008). Zinc-based glass polyalkenoate
393   cements with improved setting times and mechanical properties. *Acta Biomater,* 4(2), 425-
394   431.
395 Brady, S. A., Fox, E. K., Lally, C., & Clarkin, O. M. (2017). Optimisation of a novel glass-alginate
396   hydrogel for the treatment of intracranial aneurysms. *Carbohydrate Polymers,* 176, 227-
397   235.
398 Bragg, K., Vanbalen, N., & Cook, N. (2005). Future trends in minimally invasive surgery. *AORN
399   J,* 82(6), 1006-1014, 1016-1008; quiz 1019-1022.
400 Brook, I. M., & Hatton, P. V. (1998). Glass-ionomers: bioactive implant materials. *Biomaterials,*
401   19(6), 565-571.
402 Buwalda, S. J., Boere, K. W. M., Dijkstra, P. J., Feijen, J., Vermonden, T., & Hennink, W. E.
403   (2014). Hydrogels in a historical perspective: From simple networks to smart materials.
404   *Journal of Controlled Release,* 190, 254-273.
405 Chan, G., & Mooney, D. J. (2013). Ca2+ released from calcium alginate gels can promote
406   inflammatory responses in vitro and in vivo. *Acta Biomater,* 9(12), 9281-9291.
407 Cramer, C., Gao, Y., & Funke, K. (2005). Mixed cation effects in alkali borate glasses with varying
408   total ion concentrations. *Physics and Chemistry of Glasses,* 46(2), 90-94.
409 Dusseault, J., Tam, S. K., Menard, M., Polizu, S., Jourdan, G., Yahia, L., & Halle, J. P. (2006).
410   Evaluation of alginate purification methods: Effect on polyphenol, endotoxin, and protein
411   contamination. *Journal of Biomedical Materials Research Part A,* 76a(2), 243-251.

412 Eschenhagen, T., Didie, M., Heubach, J., Ravens, U., & Zimmermann, W. H. (2002). Cardiac
413 tissue engineering. *Transplant Immunology, 9*(2-4), 315-321.
414 Grover, G. N., Braden, R. L., & Christman, K. L. (2013). Oxime Cross-Linked Injectable
415 Hydrogels for Catheter Delivery. *Advanced Materials, 25*(21), 2937-2942.
416 Halliwell, B. (2003). Oxidative stress in cell culture: an under-appreciated problem? *Febs Letters,*
417 *540*(1-3), 3-6.
418 Haug, A., & Smidsrod, O. (1970). Selectivity of Some Anionic Polymers for Divalent Metal Ions.
419 *Acta Chemica Scandinavica, 24*(3), 843-&.
420 Henstock, J. R., Canham, L. T., & Anderson, S. I. (2015). Silicon: The evolution of its use in
421 biomaterials. *Acta Biomater, 11*, 17-26.
422 Hill, R. G., & Brauer, D. S. (2011). Predicting the bioactivity of glasses using the network
423 connectivity or split network models. *Journal of Non-Crystalline Solids, 357*(24), 3884-
424 3887.
425 Hong, S., Na, Y. S., Choi, S., Song, I. T., Kim, W. Y., & Lee, H. (2012). Non-Covalent Self-
426 Assembly and Covalent Polymerization Co-Contribute to Polydopamine Formation.
427 *Advanced Functional Materials, 22*(22), 4711-4717.
428 Jin, X. F., Xu, Y., Shen, J., Ping, Q. N., Su, Z. G., & You, W. L. (2011). Chitosan-glutathione
429 conjugate-coated poly(butyl cyanoacrylate) nanoparticles: Promising carriers for oral
430 thymopentin delivery. *Carbohydrate Polymers, 86*(1), 51-57.
431 Jork, A., Thurmer, F., Cramer, H., Zimmermann, G., Gessner, P., Hamel, K., . . . Zimmermann,
432 U. (2000). Biocompatible alginate from freshly collected Laminaria pallida for
433 implantation. *Applied Microbiology and Biotechnology, 53*(2), 224-229.
434 Kadouch, J. A., Vos, W., Nijhuis, E. W. P., & Hoekzema, R. (2015). Granulomatous Foreign-
435 Body Reactions to Permanent Fillers: Detection of CD123(+) Plasmacytoid Dendritic
436 Cells. *American Journal of Dermatopathology, 37*(2), 107-114.
437 Kjeldsen, J., Smedskjaer, M. M., Mauro, J. C., Youngman, R. E., Huang, L. P., & Yue, Y. Z.
438 (2013). Mixed alkaline earth effect in sodium aluminosilicate glasses. *Journal of Non-*
439 *Crystalline Solids, 369*, 61-68.
440 Klock, G., Frank, H., Houben, R., Zekorn, T., Horcher, A., Siebers, U., . . . Zimmermann, U.
441 (1994). Production of Purified Alginates Suitable for Use in Immunoisolated
442 Transplantation. *Applied Microbiology and Biotechnology, 40*(5), 638-643.
443 Kuo, C. K., & Ma, P. X. (2001). Ionically crosslinked alginate hydrogels as scaffolds for tissue
444 engineering: Part 1. Structure, gelation rate and mechanical properties. *Biomaterials, 22*(6),
445 511-521.
446 Lee, K. Y., & Mooney, D. J. (2012). Alginate: Properties and biomedical applications. *Progress*
447 *in Polymer Science, 37*(1), 106-126.
448 Li, J. J., Kaplan, D. L., & Zreiqat, H. (2014). Scaffold-based regeneration of skeletal tissues to
449 meet clinical challenges. *Journal of Materials Chemistry B, 2*(42), 7272-7306.
450 Messas, E., Pernot, M., & Couade, M. (2013). Arterial wall elasticity: state of the art and future
451 prospects. *Diagn Interv Imaging, 94*(5), 561-569.
452 Murayama, Y., Vinuela, F., Tateshima, S., Vinuela, F., & Akiba, Y. (2000). Endovascular
453 treatment of experimental aneurysms by use of a combination of liquid embolic agents and
454 protective devices. *American Journal of Neuroradiology, 21*(9), 1726-1735.
455 Omens, J. H. (1998). Stress and strain as regulators of myocardial growth. *Progress in Biophysics*
456 *& Molecular Biology, 69*(2-3), 559-572.

457   Ravichandran, R., Venugopal, J. R., Sundarrajan, S., Mukherjee, S., & Ramakrishna, S. (2012).
458   Minimally invasive cell-seeded biomaterial systems for injectable/epicardial implantation
459   in ischemic heart disease. *Int J Nanomedicine,* 7, 5969-5994.
460   Shelby, J. E. (1994). Alkali and Alkaline-Earth Galliosilicate Glasses. *Rare Elements in Glasses,*
461   94-9, 279-316.
462   Stamboulis, A., Law, R. V., & Hill, R. G. (2004). Characterisation of commercial ionomer glasses
463   using magic angle nuclear magnetic resonance (MAS-NMR). *Biomaterials,* 25(17), 3907-
464   3913.
465   Suzuki, Y., Nishimura, Y., Tanihara, M., Suzuki, K., Nakamura, T., Shimizu, Y., . . . Kakimaru,
466   Y. (1998). Evaluation of a novel alginate gel dressing: Cytotoxicity to fibroblasts in vitro
467   and foreign-body reaction in pig skin in vivo. *Journal of Biomedical Materials Research,*
468   39(2), 317-322.
469   Thankam, F. G., & Muthu, J. (2013). Influence of plasma protein-hydrogel interaction moderated
470   by absorption of water on long-term cell viability in amphiphilic biosynthetic hydrogels.
471   *Rsc Advances,* 3(46), 24509-24520.
472   Wilson, A. D., & Nicholson, J. W. (1993). *Acid-base cements : their biomedical and industrial*
473   *applications*. Cambridge England ; New York, NY, USA: Cambridge University Press.
474   Wren, A. W., Coughlan, A., Placek, L., & Towler, M. R. (2012). Gallium containing glass
475   polyalkenoate anti-cancerous bone cements: glass characterization and physical properties.
476   *Journal of Materials Science-Materials in Medicine,* 23(8), 1823-1833.
477   Yang, C. H., Wang, M. X., Haider, H., Yang, J. H., Sun, J. Y., Chen, Y. M., . . . Suo, Z. G. (2013).
478   Strengthening Alginate/Polyacrylamide Hydrogels Using Various Multivalent Cations.
479   *ACS Appl Mater Interfaces,* 5(21), 10418-10422.
480   Zimmermann, U., Klock, G., Federlin, K., Hannig, K., Kowalski, M., Bretzel, R. G., . . . Zekorn,
481   T. (1992). Production of Mitogen-Contamination Free Alginates with Variable Ratios of
482   Mannuronic Acid to Guluronic Acid by Free-Flow Electrophoresis. *Electrophoresis,* 13(5),
483   269-274.

484